CrystEngComm

Cite this: *CrystEngComm*, 2011, **13**, 6271

www.rsc.org/crystengcomm

PAPER

Multicomponent solids of lamotrigine with some selected coformers and their characterization by thermoanalytical, spectroscopic and X-ray diffraction methods†

Renu Chadha,*[a] Anupam Saini,[a] Poonam Arora,[a] Dharamvir Singh Jain,[b] Archi Dasgupta[c] and T. N. Guru Row[c]

Received 18th April 2011, Accepted 19th July 2011
DOI: 10.1039/c1ce05458a

The present study investigates the structural and pharmaceutical properties of different multicomponent crystalline forms of lamotrigine (LTG) with some pharmaceutically acceptable coformers *viz.* nicotinamide (**1**), acetamide (**2**), acetic acid (**3**), 4-hydroxy-benzoic acid (**4**) and saccharin (**5**). The structurally homogeneous phases were characterized in the solid state by DSC/TGA, FT-IR and XRD (powder and single crystal structure analysis) as well as in the solution phase. Forms **1** and **2** were found to be cocrystal hydrate and cocrystal, respectively, while in forms **3**, **4** and **5**, proton transfer was observed from coformer to drug. The enthalpy of formation of multicomponent crystals from their components was determined from the enthalpy of solution of the cocrystals and the components separately. Higher exothermic values of the enthalpy of formation for molecular complexes **3**, **4** and **5** suggest these to be more stable than **1** and **2**. The solubility was measured in water as well as in phosphate buffers of varying pH. The salt solvate **3** exhibited the highest solubility of the drug in water as well as in buffers over the pH range 7–3 while the cocrystal hydrate **1** showed the maximum solubility in a buffer of pH 2. A significant lowering of the dosage profile of LTG was observed for **1**, **3** and **5** in the animal activity studies on mice.

Introduction

Considerable time and funds are required for the research and development and formulation of any API that is to be delivered in a solid form.[1] Unfortunately, some potentially useful APIs administered as solids may never realize their maximum potential due to unsatisfactory bioavailability, limited by their solubility.[2] The enhanced solubility critically impacts the pharmacokinetic profile of orally delivered APIs resulting in better absorption in the gastrointestinal tract (GIT) and reduced dosage-level requirements.[3] Thus, a number of approaches have been pursued for optimizing the solubility of APIs such as preparation of solid dispersions,[4] micronization,[5] the use of surfactants,[6] polymorphs,[7] self-emulsifying formulations,[8] inclusion complexation with cyclodextrins,[9] nanocrystals[10] and the use of multicomponent molecular crystals.[11] Recently there is heightened interest and awareness of the need to diversify the range of crystal forms exhibited by APIs. The multicomponent approach that includes salts as well as cocrystals results in a set of structural variations of the same API. Salt formation indeed is a widely accepted approach to modify the physical properties of APIs,[12–17] however, pharmaceutical cocrystallization is a relatively recent technology which offers an alternative platform to improve the physicochemical properties of active pharmaceutical ingredients (APIs), such as the melting point, solubility, stability, and dissolution rate.[18–26] Pharmaceutical cocrystals, multiple component solids, also represent a broad patent space since they are clearly new chemical entities, and their design and preparation involve several elements of non-obviousness and they generally have novel and useful properties.[27]

Lamotrigine (LTG) [3,5-diamino-6-(2,3-dichlorophenyl)-1,2,4-triazine] is an anticonvulsant drug having poor solubility in water (0.17 mg mL^{-1} at 25 °C)[28] which limits its absorption and dissolution rate and thus delays the onset of action.[29] Thus, there is a need to develop alternative forms of LTG with improved solubility which can significantly enhance the oral absorption of this drug in GIT. The LTG framework is comprised of four acidic amino hydrogen bond donors along with two basic hydrogen bond acceptors *i.e.* amino-pyridine nitrogen atoms giving rise to a variety of hydrogen bonding donor/acceptor sites for an approaching coformer to bind, thus making it a potential target for both cocrystal and salt formation. These features of LTG along with the availability of a vast number of coformers of GRAS (Generally Regarded As Safe) status[30] for cocrystallization

[a]*University Institute of Pharmaceutical Sciences, Panjab University, Chandigarh, 160014, India. E-mail: renukchadha@rediffmail.com; Tel: +91-9316015096*
[b]*Department of Chemistry, Panjab University, Chandigarh, 160014, India*
[c]*Solid State and Structural Chemistry Unit (SSCU), Indian Institute of Science, Bangalore, 560012, India*

† CCDC reference numbers 791931, 819591 and 819592. For crystallographic data in CIF or other electronic format see DOI: 10.1039/c1ce05458a

persuaded us to explore this multicomponent approach in an attempt to enhance the solubility of this anticonvulsant drug. Various groups of researchers have worked on LTG crystal forms and have reported solvates,[31–37] salts[38–42] and cocrystals[42] of this drug. One of the recent reports is by Galcera and Molins[41] on LTG salts with four different counter-ions such as succinic acid, fumaric acid, DL-tartaric acid and saccharin, of which only saccharinate and DL-hemitartrate dimethylsulfoxide solvates exhibited higher aqueous solubility than the pure drug. However, the use of dimethylsulfoxide as a solvent is not safe for human consumption. Beside this, Cheney *et al.*[42] reported cocrystals of LTG with methylparaben and nicotinamide and salts with saccharin, adipic acid, malic acid and nicotinic acid in 2010. The solubility and pharmacokinetic studies on only a few of these forms have been reported and revealed that only the saccharinate salt of LTG exhibited substantial improvement in these targeted properties. In the present work, multicomponent forms of LTG with nicotinamide, acetamide, acetic acid, 4-hydroxy-benzoic acid and saccharin are reported. Most of these coformers have been selected based on their pK_a value with an intention to obtain intermolecular hydrogen bonded complexes with LTG. Except for the cocrystal hydrate of LTG with nicotinamide and the salt of LTG with saccharin, none of the other forms described in this work have been reported earlier. Despite the fact that LTG-saccharinate had already been reported[41] this coformer was selected in the present work because of its additional advantages such as a sweetening agent, low toxicity and appreciable water solubility.[15] Although the first characterization of LTG-nicotinamide monohydrate and LTG-saccharin salt has already been reported by Cheney *et al.*,[42] we incorporated their findings in the present work for comparison and found our results to be in good agreement with their reports. In addition, a few additional parameters such as the enthalpy of solution as well as stability studies which are missing in the literature have been included in the present study. The characterization was done using differential scanning calorimetry (DSC), thermogravimetric analysis (TGA), Fourier transform infra-red spectroscopy (FT-IR) and X-ray diffraction (XRD) analysis, which confirmed that two of these forms are cocrystals and the remaining three are salts. Beside this, the technique of solution calorimetry has also been utilized to give an insight into the breaking of the lattice of these multicomponent crystals upon dissolution. Further, the solubility, stability and animal activity studies using the mouse maximal electroshock (MES) model[43] were performed on these multicomponent forms.

Experimental

LTG was obtained as complimentary sample from Rantus Pharma Pvt. Ltd. (India). The guest compounds and crystallization solvents were of AR grade and purchased from various commercial suppliers. All of these were used as received.

Sample preparation

LTG-nicotinamide monohydrate (1). Compound **1** was prepared by the solvent evaporation method. A stoichiometric amount of LTG (0.256 g, 1 mmol) and nicotinamide (0.122 g, 1 mmol) were added to 5 mL methanol followed by stirring at 50 °C for 2 hours. The clear solution was evaporated rapidly under vacuum, and then the crystalline solid obtained was scraped from the walls of the flask and stored in an airtight glass vial. The attempts to produce single crystals of **1** as described by Cheney *et al.*[42] resulted in the re-crystallization of the starting components individually, may be due to different laboratory temperature conditions.

LTG-acetamide (2). The co-crystallization was performed by the reaction crystallization method by adding LTG (0.2 g, 0.78 mmol) to 4 mL of presaturated isobutanol solution of acetamide and keeping at room temperature for slow evaporation. The crystals of compound **2** of size suitable for single crystal XRD were obtained, filtered, air dried and stored in airtight glass vials.

LTG-acetic acid (3). Single crystals of **3** were obtained by dissolving LTG in an excess of acetic acid with heat and evaporating slowly.

LTG-4-hydroxy-benzoic acid (4). LTG (0.128 g, 0.49 mmol) was added to 3 mL of ethanol and dissolved by warming. To this clear solution, an ethanolic solution of 4-hydroxybenzoic acid (0.069 g, 0.49 mmol) was added producing instantaneous precipitation of a fine powder of compound **4** which was filtered, air dried and stored in a vial. Single crystals of **4** were obtained by slow evaporation of the filtrate.

LTG-saccharin (5). LTG (0.758 g, 2.9 mmol) was added to 50 mL solution of saccharin (0.549 g, 2.9 mmol) in acetonitrile and dissolved with slight warming until the dissolution was complete. The clear solution was allowed to slowly evaporate at room temperature. Single crystals of **5** were obtained within a few hours.

Characterization of crystals in the solid state

Differential scanning calorimetry (DSC). Differential scanning calorimetry of all the samples was conducted using a DSC Q20 (TA Instruments, USA). The samples (3–5 mg) were placed in sealed non-hermetic aluminium pans and were scanned at a rate of 5 °C min^{-1} in the range of 25–300 °C under a dry nitrogen atmosphere (flow rate 50 mL min^{-1}). The data were managed by TA Q series Advantage software (Universal analysis 2000).

Thermogravimetric analysis (TGA). TGA was performed using a Mettler Toledo TGA/SDTA 851^e instrument. Approximately 5 mg sample was heated from 25 to 300 °C in an open alumina pan at the rate of 10 °C min^{-1} under nitrogen purge at a flow rate of 50 mL min^{-1}. The data were managed by STAR software (9.00).

Hot stage microscopy. Melting points and physical changes were visually examined at 50× magnification by hot stage microscopy. The study was carried out using an optical/polarized hot stage microscope (Leica DMLP, Leica, Germany) equipped with a controlled heating and cooling stage (LTS350, Linkam) and an imaging system (VTO 232, JVC-Digital camera and Linksys 32 imaging software, Linkam, England). The powder sample was mounted in air and heated from 25 °C to 230 °C at a rate of 5 °C min^{-1}.

X-Ray powder diffraction (XRPD). XRPD patterns were collected using an X'Pert PRO diffractometer system (Panalytical, Netherlands) with a Cu Kα radiation (1.54060 Å). The tube voltage and current were set at 45 kV and 40 mA respectively. The divergence slit and anti-scattering slit settings were set at 0.48° during illumination on the 10 mm sample size. Each sample was packed in an aluminium sample holder and measured by a continuous scan between 5 and 50° in 2θ with a step size of 0.017°. The experimental XRPD patterns were refined using X'Pert High Score software.

Fourier transform-infrared spectroscopy (FT-IR). A Spectrum RX I FT-IR spectrometer (Perkin Elmer, UK) was employed in the KBr diffuse-reflectance mode (sample concentration 2 mg in 20 mg of KBr) for collecting the IR spectra of samples. The spectra were measured over the range of 4000–400 cm^{-1}. Data were analyzed using Spectrum software.

Single crystal X-ray diffraction. The X-ray diffraction dataset for compound **2** was collected on an Oxford Xcalibur (Mova) diffractometer[44] equipped with an EOS CCD detector using Mo-Kα radiation (λ = 0.71073 Å) at room temperature. X-Ray diffraction datasets for compounds **3** and **4** were collected on a Bruker AXS Kappa Apex CCD diffractometer using Mo-Kα radiation at 90 K. All structures were solved by direct methods using SHELXS-97 and refined against F^2 using SHELXL-97.[45] The hydrogen atoms in carboxylic acid groups and amide groups associated with the formation of either a salt or a cocrystal of lamotrigine were located based on the difference Fourier map and were refined isotropically. All other hydrogen atoms were placed geometrically and refined with an isotropic displacement parameter fixed at 1.2 times U_q of the atoms to which they were attached. The WINGX package (version1.70.01)[46] was used for refinement and production of data tables and ORTEP-3[47] for structural visualization. All ORTEP representations were made using POV-Ray[48] showing ellipsoids at the 50% probability level. Analysis of the H-bonding and other non-covalent interactions was carried out using PARST95 and PLATON[49] for all the structures. Packing diagrams were generated using Mercury-2.2.[50]

Analysis in the solution phase

Solution calorimetry studies. The enthalpy of solution of the drug, coformers and the multi-component forms was determined using a Micro Reaction Calorimeter (a power compensation system) obtained from Thermal Hazards Technology (UK) in a phosphate buffer at pH 7.0 and 37 °C. Two experimental vials (reference and sample) filled with an equal volume of buffer were placed in a calorimetric block. A solid sample of about 1 to 2 mg, accurately weighed (Sartorius Model CP225D), was loaded into a cylindrical glass tube (solid sample insert) covered with parafilm on one side and submerged into the sample vial. After baseline stabilization at 37 °C (±0.0005 °C), the sample was released into the sample vial by means of a plunger. The heat output was recorded and integrated to calculate the enthalpy of solution. The precision of any individual measurement was better than 0.02 kJ mol^{-1}, for three consecutive experiments and agreed with the standard value within ±0.03 kJ mol^{-1}. In the case of liquid samples like acetic acid, the enthalpy of solution in buffer was determined using the titration mode of the Micro Reaction Calorimeter. The reference and sample vials filled with an equal volume of buffer were placed in a calorimetric block set at 37 °C. A 100 μl syringe loaded with acetic acid was mounted on the sample vial. After baseline stabilization, 50 μl of the acid was injected into the sample vial and the heat output was recorded and integrated to calculate the enthalpy of solution.

Equilibrium solubility studies. Solubility of the LTG free base and compounds **1–5** has been determined in water at various time points to ensure that the solution has reached equilibrium. For this study, the starting solids were sieved using a Gilson mesh sieve to provide samples with an approximate particle size of 150 μm. In each experiment, a flask containing 50 mL of water was equilibrated at 37 °C in a constant temperature bath. An excess of solid phase (*ca.* 50 mg) was added to the flask and the resulting slurry was shaken at 200 rpm. An aliquot of slurry was withdrawn at multiple time points, filtered through a 0.45 μm membrane filter, diluted suitably and the concentration was determined spectroscopically by measuring the absorbance at 305 nm with a Lambda 25 UV/VIS spectrometer. The extinction coefficient of LTG was obtained through calibration experiments carried out in pure water (ε_{305} = 6.8 × 10^3 M^{-1} cm^{-1}). For experiments involving compounds **1–5**, the absorbance values were related to solution concentrations using their respective calibration curves in their respective medium. This was possible since none of the coformers absorb at 305 nm and therefore did not interfere with determination of the concentration of LTG. After the last aliquot was collected, the remaining solids were filtered, air dried and analyzed by XRPD. The equilibrium solubility of LTG free base and compounds **1–5** has also been determined in phosphate buffers of pH 7, 5, 3 and 2. As the pK_a of LTG is 5.7, there is a possibility that after dissolution it may be present in the solution in either its protonated or unprotonated form depending upon the pH of the solution. The concentration was determined at λ corresponding to an isosbestic point of LTG (288 nm).

Stability studies. Accurately weighed samples (approximately 100 mg) placed in loosely capped glass vials were kept in a stability chamber at 25 °C/60% RH for one month and then analyzed by XRPD.

Animal activity studies. Male mice (Balb/C, 20–30 g) were used. Animals were weighed and placed in standard cages with free access to food and tap water. After 7 days of adaptation to laboratory conditions, the animals were randomly assigned to experimental groups each comprising 6 mice. LTG free base and compounds **1–5** were prepared as suspensions in 0.5% carboxymethylcellulose in saline and administered *via* oral gavage. After 15 minutes of drug dosing, electroconvulsions were produced by current (fixed current 30 mA, stimulus duration 0.2 s) delivered to saline-wetted eyes *via* corneal electrodes from an electroshock apparatus (IMCORP, India). The criterion for the occurrence of seizure activity was the tonic hind limb extension (HLE *i.e.*, the hind limbs of animals outstretched 180° to the plane of the body axis). The protective activity of LTG free base and its multi-component forms was determined as the median effective dose

(ED_{50} value in mg kg^{-1}) against maximal electroshock (MES) induced seizures. Sufficient animals were tested over the range of four different doses of each compound (2.5, 5.0, 7.5 and 10.0 mg kg^{-1} of LTG or its equivalent) to provide data for calculation of ED_{50} values. The data were processed using the Microsoft Office Excel 2007 software package. This experiment is approved by the Institutional Animal Ethical Issue Committee and has been conducted according to Indian National Science Academy (INSA) guidelines for use and care of experimental animals.

Results and discussion

LTG has the ability to form both salts and cocrystals due to its relatively basic nature ($pK_a = 5.7$). The pK_a difference between the drug and coformer (ΔpK_a) can give an idea about the formation of salt or cocrystal. In general, a higher ΔpK_a (greater than 3) will result in salt formation while a lower ΔpK_a (less than 0) will almost exclusively result in cocrystal formation.[51] However, in the range 0 to 3, the complexes between acids and bases can be salts or cocrystals or may contain shared protons or mixed ionization states that cannot be assigned to either category. The pK_a values of coformers involved in this study are summarized in Table 1. Based on the ΔpK_a values, acetamide has a high probability of forming a cocrystal, saccharin is expected to give a salt only, while the remaining three coformers may result in cocrystal or salt formation with LTG. Thus, the forms obtained in these cases have to be ascertained by various techniques. Melting points and shapes of crystals of various phases

Table 1 pK_a Values of LTG and coformers and the resulting ΔpK_a values for the LTG multicomponent forms

Compound	pK_a	ΔpK_a (pK_a base − pK_a acid)
LTG (free base)	5.70	—
Nicotinamide	3.35	2.35
Acetamide	17.00	−11.3
Acetic acid	4.80	0.90
4-Hydroxy-benzoic acid	4.48	1.22
Saccharin	2.32	3.38

Table 2 Melting point and morphology of LTG free base and compounds **1–5**

Compound	Mp/°C	Morphology of crystals
LTG	216–217	Rectangular blocks
1	169–173	Irregular shape
Nicotinamide	128–131[a]	—
2	159–160	Rectangular blocks
Acetamide	78–81[a]	—
3	149–170	Rectangular blocks
Acetic acid	16.64 (mp)[a], 118 (bp)[a]	—
4	232–234	Rhombus shape
4-Hydroxy-benzoic acid	213–216[a]	—
5	255–257	Rectangular blocks
Saccharin	228–229[a]	—

[a] Obtained from Merck Index.

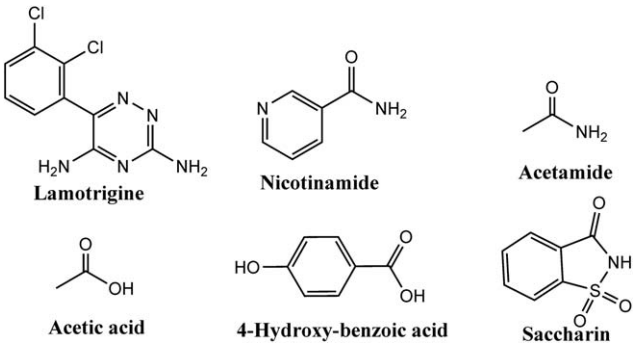

Scheme 1 Molecular structures of Lamotrigine and coformers.

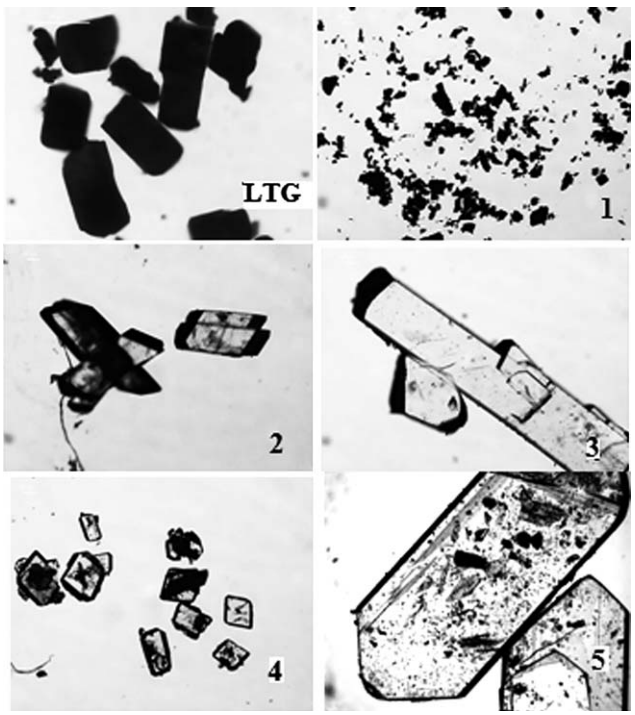

Fig. 1 Optical micrographs of compounds **1–5**.

are given in Table 2. The difference in melting points of these compounds and their individual components strongly indicates the formation of phases that are unique to their starting components. These solid phases, formed with nicotinamide **1**, acetamide **2**, acetic acid **3**, 4-hydroxy-benzoic acid (4-HBA) **4** and saccharin **5**, were characterized in both the solid state and the solution form. The molecular structures of LTG as well as all the coformers are given in Scheme 1 and the morphology of all these forms is shown in Fig. 1.

Characterization in the solid state

Thermal analysis utilizing DSC, TGA and hot stage microscopy. DSC and TGA scans of LTG and compounds **1–5** are shown in Fig. 2 and 3 respectively. The DSC thermogram of LTG showed a single melting endotherm at 217.1 °C. A broad endotherm was observed in the DSC thermogram of **1** with an onset at 80.7 °C followed by a sharp endothermic peak at

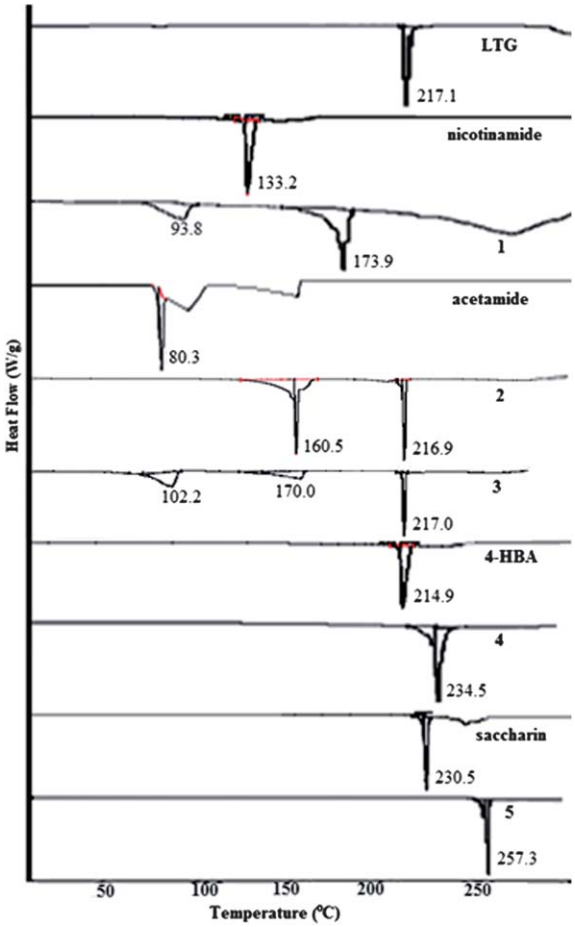

Fig. 2 DSC thermograms of LTG free base and its multicomponent forms **1**–**5**.

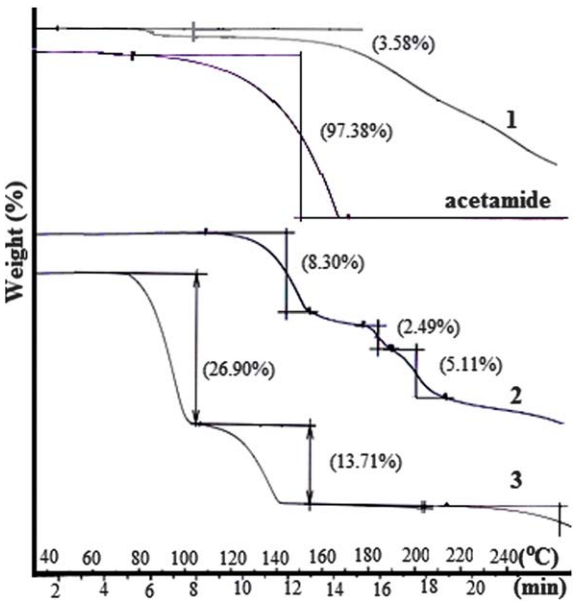

Fig. 3 TGA curves of compounds **1**, **2**, **3** and acetamide.

173.9 °C which is different from melting peaks of both LTG and nicotinamide (133.2 °C). The DSC scan of a binary mixture of the starting components exhibited two different endotherms corresponding to their melting thus ruling out the probability of any eutectic formation. A TGA scan of **1** showed a weight loss of 3.58% (in the range of 80–100 °C) which correlates to the loss of a single water molecule (theoretical weight loss of 4.54%). This suggests that **1** is a monohydrate. This is further confirmed by comparison of our results with those of Cheney *et al.*[42] which showed a slight variation in the desolvation peak (onset at 90.0 °C[42]) whereas the melting endotherm (174.8 °C[42]) is approximately the same. The difference in the onset of the desolvation peak may be due to the difference in the rate of scanning. Similarly the % loss in TGA is also in good agreement (3.74%[42]). These thermoanalytical results supported by those of Cheney *et al.*[42] suggest **1** to be the monohydrate cocrystal of LTG with nicotinamide.

Two major endothermic events were observed in the DSC scan of **2**. A broad endotherm at 160.5 °C depicting the melting of cocrystal is associated with a weight loss in the TGA. This is probably due to sublimation of the coformer (acetamide) from the melt as the TGA scan of pure acetamide also shows a similar weight loss in its melting range. Interestingly, this first broad peak is followed by a sharp endothermic peak at 216.9 °C depicting the melting of pure drug which might have appeared due to recrystallization of free base after the loss of coformer from the cocrystal melt. To have an insight into the thermal events taking place during the melting of this cocrystal resulting

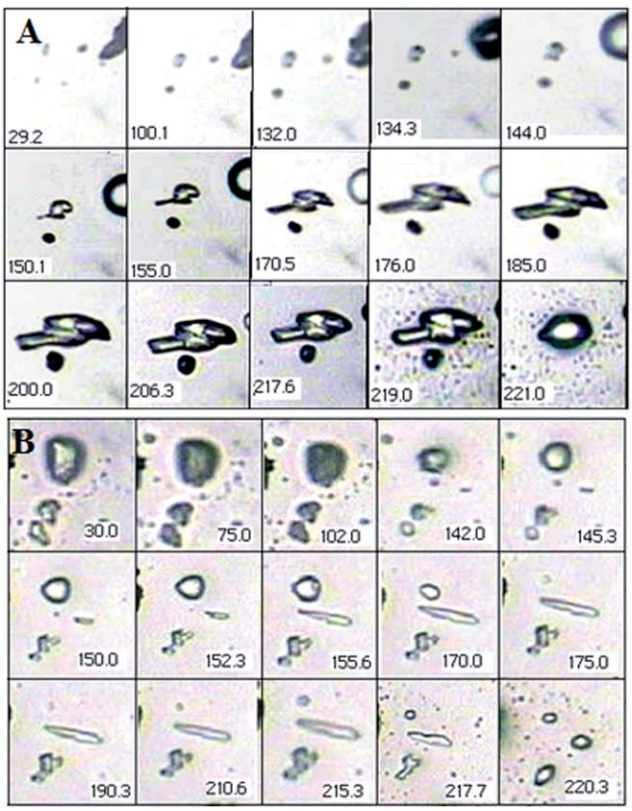

Fig. 4 Hot stage microscopy micrographs of (A) cocrystal **2** and (B) salt solvate **3**.

in the emergence of drug, hot stage microscopy was performed. As can be seen in Fig. 4A, there is no change in the crystals of **2** up to 132.0 °C. The melting of the cocrystal began at 134.3 °C and the recrystallization of LTG from this melt started at 155.0 °C. These crystals of LTG continued to grow up to a temperature of 185.0 °C and finally started melting at 219.0 °C. The occurrence of both the endothermic event due to melting of the cocrystal and the exothermic event due to recrystallization of the pure drug from this melt in the same temperature range (134–185 °C) resulted in an overall broad endothermic peak in this region in the DSC thermogram.

The DSC scan of **3** showed two broad endotherms followed by a sharp melting endotherm. The first two broad endotherms are accompanied by a weight loss in TGA in temperature ranges of 75–110 °C (26.9%) and 115–170 °C (13.7%) respectively. The two step weight loss in TGA is attributed to evaporation of overall three molecules of acetic acid released in two steps. The broad peak in the DSC at 102 °C is attributed to desolvation and the stoichiometric calculation (theoretical weight loss of 27.5%) shows the release of two molecules of acetic acid. The second broad endotherm at higher temperature (170 °C) indicates the phase transition leading to the melting of the multicomponent crystal with simultaneous release of one molecule of acetic acid from the crystal lattice as suggested by the theoretical weight loss of 13.8%. The emergence of sharp melting endotherm at 217.0 °C suggests the transformation of the original crystal lattice of **3** after the evaporation of three acetic acid molecules to pure LTG. This was supported by various events observed during hot stage microscopy. Fig. 4B shows that the crystals became opaque in the temperature range of 75–102 °C suggesting the loss of acetic acid molecules present as solvent in these crystals as indicated by DSC and TGA. These desolvated crystals started melting at 142.0 °C. A sequence of images shows simultaneous recrystallization of LTG from the melt. Upon further heating, the size of melt droplets decreased while the crystals of LTG continued growing up to 175.0 °C with no further change until final melting at 220.3 °C. Thus, we can say that the exothermic peak due to recrystallization of LTG has merged with the broad endothermic peak due to melting of desolvated crystals of **3** in the DSC scan. Therefore, DSC results suggest **3** to be a multicomponent crystal of LTG and acetic acid with 1 : 3 stoichiometry.

DSC scans of **4** and **5** showed single, sharp melting endotherms at 234.5 and 257.3 °C respectively, which are at a higher temperature than LTG as well as the respective coformers (4-HBA = 214.9 °C and saccharin = 230.5 °C). These also indicate the absence of any eutectic formation as eutectics melt at temperatures between those of the melting points of the starting components. The melting peak of **5** has been found to be in good agreement with that of the LTG-saccharin salt reported by Galcera and Molins[41] (256.0 °C), however, there is slight variation from that reported by Cheney *et al.*[42] (252.5 °C). Further, TGA of both **4** and **5** did not reveal any weight loss indicating the existence of anhydrous and stable phases unique to their starting components. Thus, DSC/TGA has shown the existence of multicomponent crystals of LTG with various coformers which are present in different stoichiometry.

XRPD analysis. Compounds **1–5** displayed unique crystalline XRPD patterns in comparison to LTG and their respective coformers indicating the generation of new solid phases. These unique peaks corresponding to each of the molecular complexes are shown in Fig. 5A. The experimental powder pattern of compound **1** was compared with the simulated XRPD pattern generated from the previously determined single crystal data of both LTG-nicotinamide cocrystal monohydrate as well as the LTG-nicotinamide cocrystal (anhydrous).[42] It is clear from Fig. 5B that the XRPD pattern of compound **1** correlates nicely to the simulated pattern of LTG-nicotinamide cocrystal monohydrate rather than its anhydrous form, thus, confirming **1** to be identical to the known hydrate form. Similarly, the powder pattern of compound **5** is compared with the simulated pattern derived from the known crystal structure of LTG-saccharin salt[42] and the two are found to be identical (Fig. 5B), thus, confirming compound **5** to be LTG-saccharin salt. No prior data are available for comparison of XRPD patterns of compounds **2–4**. Although formation of new solid phases in **2**, **3** and **4** has been identified by a combination of DSC/TGA and XRPD analysis, the transfer of protons in these solids was ascertained only by FTIR spectroscopy and single crystal X-ray diffraction studies.

FT-IR. FTIR spectroscopy is an excellent technique to characterize and distinguish cocrystals from salts, especially when a carboxylic acid is used as a coformer. LTG shows an IR absorption frequency for a primary amine N–H stretch at 3448 and 3316 cm^{-1}, a C–H aromatic stretch at 3209 cm^{-1} and a primary amine N–H bend at 1620 cm^{-1} (Fig. 6). In the FTIR spectra of **1**, the amino N–H stretch of LTG shifted to 3413 and 3325 cm^{-1} while the N–H and C=O stretches of the amide group of nicotinamide at 3160 and 1680 cm^{-1} shifted to 3145 and 1692 cm^{-1}, respectively suggesting that both these components are participating in certain kinds of interactions. The IR spectrum of compound **1** is in good agreement with that reported by Cheney *et al.*[42] By combining these results with DSC/TGA and XRPD findings, compound **1** can be identified as a cocrystal hydrate of LTG with nicotinamide. In the FTIR spectra of **2**, the N–H stretch of the amine base of LTG at 3448 cm^{-1} and the amide function of acetamide at 3347 cm^{-1} shifted to 3424 and 3327 cm^{-1} respectively while the C=O stretch of the acetamide shifted from 1676 to 1650 cm^{-1} demonstrating interactions between these groups of LTG and acetamide. Similarly, these changes were also observed in multicomponent crystal **3**. The coformer acetic acid being an aliphatic carboxylic acid absorbs at 1715 cm^{-1} corresponding to the C=O stretch. This absorption moves to a lower wavenumber if the oxygen atom attached to carbonyl is ionized and this is evident in the IR spectra of **3** which exhibits a band at 1687 cm^{-1} corresponding to carboxylate stretching in addition to the significant shift of the NH stretch of the amine base of LTG suggesting it to be the LTG salt. Compounds **4** and **5** also showed characteristic broad bands between 3300 and 2000 cm^{-1} corresponding to $N–H^+$ signals of amine hydrogen bonded salts (absent in spectra of drug) suggesting these to be salts of LTG. Further, the shifting of carboxylic acid C=O stretch from 1677 and 1721 cm^{-1} to lower wavenumbers of 1664 and 1678 cm^{-1} in **4** and **5**, respectively clearly indicates salt formation. In addition, the IR spectrum of **5** was found to be identical to that of LTG saccharinate provided by M. L. Cheney *et al.*,[52] thus confirming the two to be the same.

Crystal structure analysis. The single crystal structures of **1** (LTG-nicotinamide hydrate) and **5** (LTG-saccharin salt) have been published previously by M. L. Cheney *et al.*[42] The crystal structure of LTG[42] is built from hydrogen bonded dimeric units of the drug molecule showing two dominant supramolecular synthon motifs, the aminopyridine dimer (motif 1) and the amine–aromatic nitrogen synthon (motif 2). The LTG dimer homosynthon is conserved in complexes **2–4** as well except for slight deviations in the geometry of LTG dimer which is formed through three different parts of the LTG molecule, N3 and N2

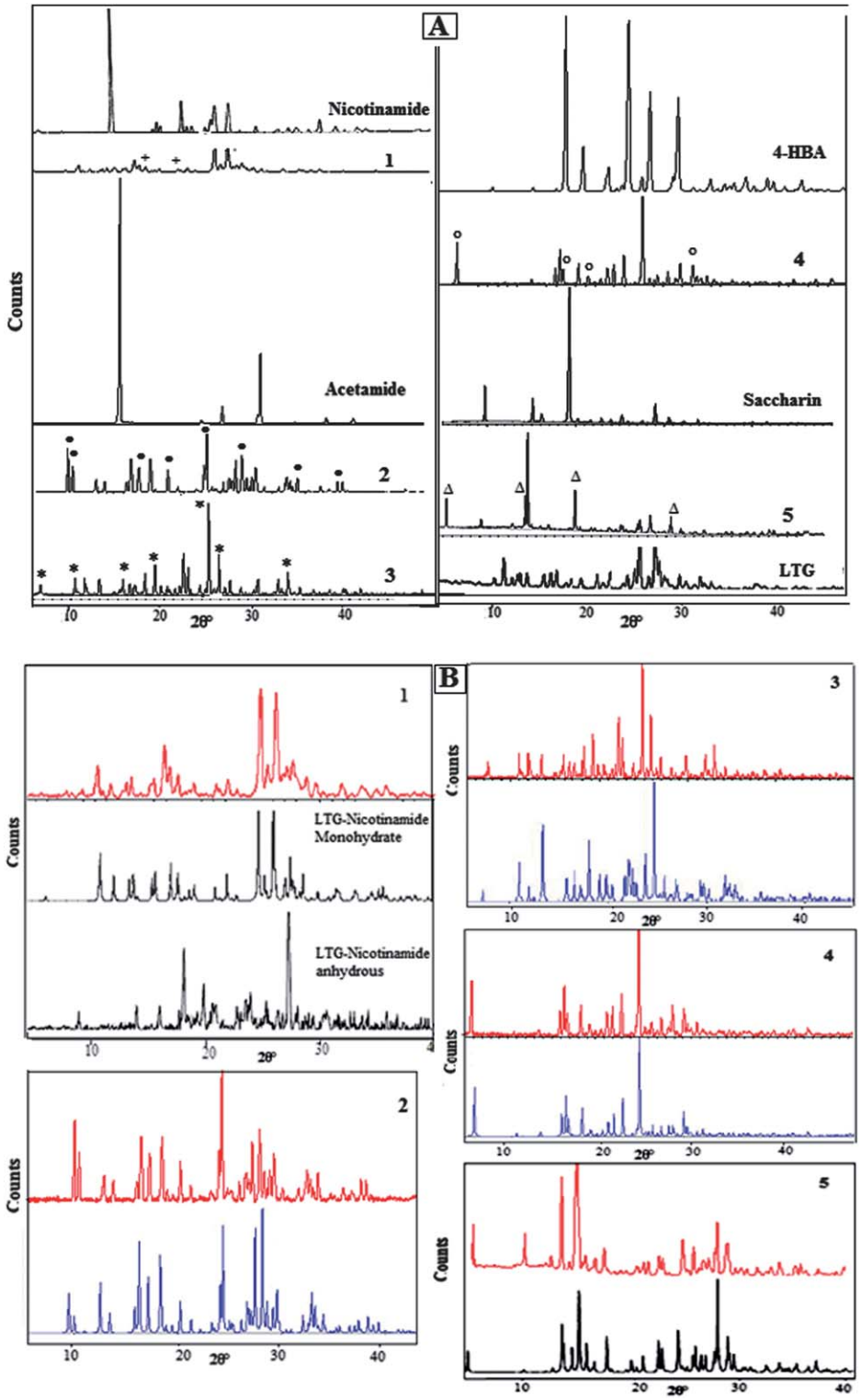

Fig. 5 (A) XRPD patterns of LTG free base, coformers and their multicomponent forms **1–5**. (B) Experimental XRPD patterns (red) of compounds **1–5** compared with their Rietveld refined simulated XRPD patterns (blue/ black).

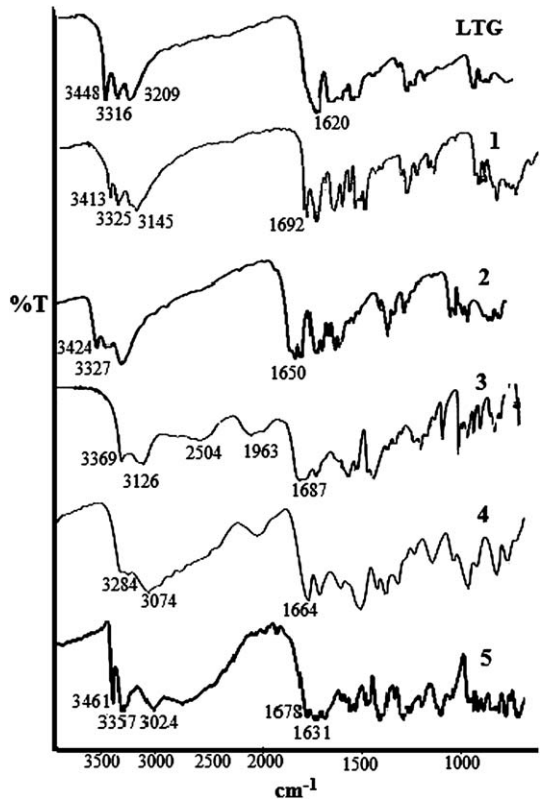

Fig. 6 FT-IR spectra of LTG free base and its multicomponent forms **1–5**.

(motif 1), N4 and N3 (motif 3) or N1 and N2 (motif 4). The possible reason for these geometry changes is that the other hydrogen bonding interactions that come up due to incorporation of the coformer are stronger as compared with the original drug. However, in all these three complexes (**2–4**), the incorporation of complementary coformer breaks motif 2. Fig. 7 represents the four different hydrogen bond motifs. Crystallographic data, *D*c–o distances (*i.e.* carbon oxygen distances in the acid carbonyl group) and hydrogen bond geometries of compounds **2–4** are given in Tables 3, 4 and 5 respectively. The simulated XRPD patterns of compounds **2–4** generated from their single crystal data are compared with their experimental XRPD patterns and found to be identical (Fig. 5B).

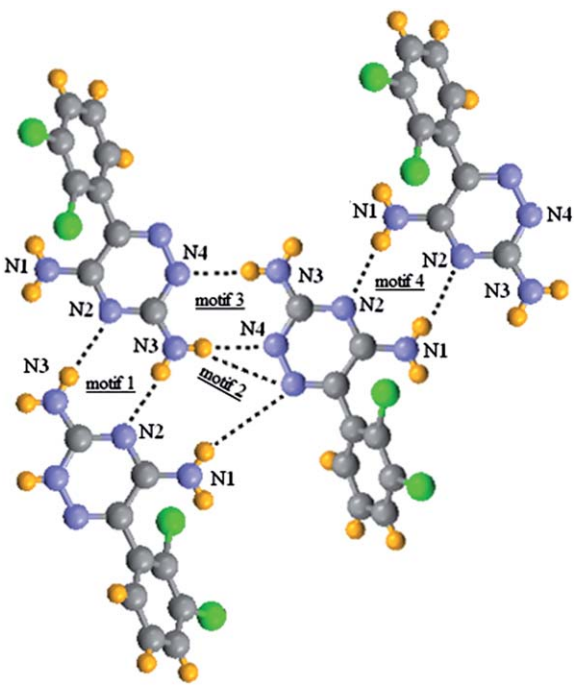

Fig. 7 Scheme representing all the four hydrogen bonding motifs.

(2) LTG-acetamide cocrystal (1 : 1). Complex **2** crystallizes in the space group $P\bar{1}$ with the asymmetric unit consisting of one molecule of LTG and one molecule of acetamide (Fig. 8). Both LTG and acetamide remain neutral in the crystal lattice of **2** and hence complex **2** is a cocrystal. The basic supramolecular unit is comprised of a LTG dimer homosynthon (N3–H3A···N4, N···N 3.070(3) Å, N···H 2.256(2) Å, N–H···N 157.9(2)°) and an acetamide dimer homosynthon (N6–H6B···O1, N···O 2.962(5) Å, O···H 2.25(5) Å, N–H···O 170(6)°). The two dimeric motifs are linked together through the N–H···O hydrogen bond (N1–H1B···O1, N···O 2.870(4) Å, O···H 2.146(3) Å, N–H···O 141.6 (2)°) resulting in a chain along the *c*-axis. Additionally, the chains are held together by type I *trans* chlorine–chlorine interactions (Cl···Cl 3.354(2) Å, $\theta_1 = 147.1°$ and $\theta_2 = 147.0°$)[53] (Fig. 9A and B). It is of interest to note that the LTG homosynthon dimer in compound **2** involves motif 3 unlike motif 1 in the reported crystal structure of LTG.[42]

Table 3 Crystallographic data for multicomponent crystals **2–4**

Parameters	**2**	**3**	**4**
Formula	$C_9H_7Cl_2N_5$, C_2H_5NO	$C_9H_8Cl_2N_5$, $2(C_2H_4O_2)$, $C_2H_3O_2$	$C_9H_8Cl_2N_5$, $C_7H_5O_3$
Stoichiometry	1 : 1	1 : 3	1 : 1
Crystal system	Triclinic	Monoclinic	Monoclinic
Space group	$P\bar{1}$	$P2_1/c$	$P2_1/c$
a/Å	7.7752(3)	7.0795(3)	15.5808(10)
b/Å	9.6284(4)	17.7124(7)	9.6890(6)
c/Å	10.4511(3)	15.9227(7)	11.1057(7)
α/deg	106.390(3)	90.000(0)	90.000(0)
β/deg	107.730(3)	94.618(2)	91.312(3)
γ/deg	101.093(3)	90.000(0)	90.000(0)
Volume/Å^3	680.98(5)	1990.14(14)	1676.10(18)
Calc. density/g cm^{-3}	1.537	1.456	1.562
Z	2	4	4
R-Factor (%)	5.46	3.01	3.71
T/K	293(2)	90(2)	90(2)

Table 4 Distribution of C–O bond lengths for multicomponents formed with carboxylic acids

Compound	Coformer	*D*c–o/Å	Δ*D*c–o/Å
3	Acetic acid	1.310(2), 1.220(2) (Dc_{10}–o_3, Dc_{10}–o_4)	0.090
		1.311(2), 1.222(2) (Dc_{12}–o_1, Dc_{12}–o_2)	0.099
		1.258(2), 1.261(2) (Dc_{14}–o_5, Dc_{14}–o_6)	0.003
4	4-Hydroxybenzoic acid	1.283(2), 1.261(3) (Dc_{16}–o_1, Dc_{16}–o_2)	0.022

Table 5 Geometrical parameters of hydrogen bonds in compounds **2–4**

D–H···A	Symmetry	*r* (H···A)/Å	*r* (D···A)/Å	*r* (D–H)/Å	∠D–H···A/°
Compound ***2***					
N1–H1B···O1	$-x+1, -y+1, -z+1$	2.146(3)	2.870(4)	0.860(2)	141.6(2)
N6–H6B···O1	$-x, -y+1, -z+1$	2.25(5)	2.962(5)	0.72(5)	170(6)
N3–H3A···N4	$-x+1, -y, -z-1$	2.256(2)	3.070(3)	0.860(2)	157.9(2)
N6–H6A···N4	$-x+1, -y+1, -z$	2.54(6)	3.383(6)	0.87(6)	164(5)
Compound ***3***					
N1–H1A···O2	$x-1, +y, +z$	1.969(1)	2.808(2)	0.860(1)	164.5(1)
O3–H3O···O5	$x+1, +y, +z$	1.69(3)	2.553(2)	0.87(3)	167(3)
N1–H1B···O4	x, y, z	2.040(1)	2.840(2)	0.860(1)	154.4(1)
N4–H4A···O5	$x, -y+1/2, +z-1/2$	1.87(2)	2.719(2)	0.89(2)	159(2)
N3–H3A···N2	$-x+2, -y, -z+1$	2.284(1)	3.137(2)	0.860(1)	171.6(1)
O1–H1O···O6	$-x+1, +y-1/2, -z+1/2+1$	1.47(3)	2.509(2)	1.04(3)	175(3)
Compound ***4***					
N4–H4A···O1	$-x+1, -y+1, -z+1$	1.79(3)	2.692(2)	0.90(3)	176(3)
N3–H3A···O1	$-x+1, +y+1/2, -z+1/2$	2.194(1)	3.001(2)	0.860(2)	156.1(1)
O3–H3O···O2	$-x-1, +y-1/2, -z+1/2$	1.830(1)	2.642(2)	0.820(2)	170.1(1)
N1–H1A···N2	$-x+1, -y+2, -z+1$	2.063(2)	2.910(3)	0.860(2)	168.1(1)
N1–H1B···O1	$-x+1, -y+1, z+1$	2.427(1)	2.977(2)	0.860(2)	122.3(1)
N3–H3B···O2	$x, -y+1/2+1, +z+1/2$	1.879(2)	2.713(2)	0.860(2)	163.0(1)

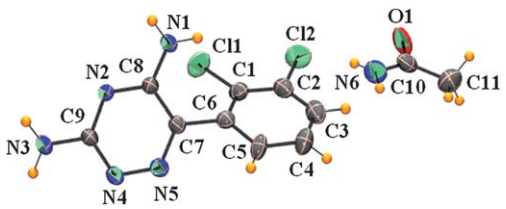

Fig. 8 ORTEP diagram of the asymmetric unit of cocrystal **2** with 50% thermal ellipsoid probability.

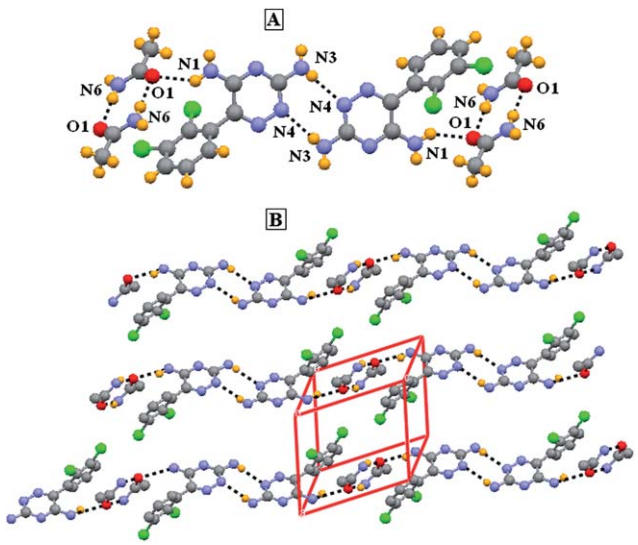

Fig. 9 (A) Hydrogen bonding scheme of **2**. (B) Packing diagram of **2** (showing hydrogen bonding and Cl···Cl interactions).

*(**3**) LTG-acetic acid salt solvate (1 : 3).* Complex **3** crystallizes in a monoclinic space group $P2_1/c$. The asymmetric unit consists of one LTG cation, two molecules of acetic acid and one acetate anion. Hence this complex can be called a 1 : 1 salt of LTG and acetic acid along with two neutral acetic acid solvent molecules in the asymmetric unit (Fig. 10). An acetic acid trimeric homosynthon ((O3–H3O···O5, O···O 2.553(2) Å, O···H 1.69(3) Å, O–H···O 167(3)°), (O1–H1O···O6, O···O 2.509(2) Å, O···H 1.47(3) Å, O–H···O 175(3)°)) generates a layer motif perpendicular to the *c* axis (Fig. 11A). In this trimer, one of the acetic acid molecules transfers a proton to LTG, which is seen from the nearly equal bond distances associated with the C–O moiety. Indeed, the Δ*D*c–o of 0.003 Å for this acetic acid molecule (Table 4) is much smaller when compared to the values of Δ*D*c–o of 0.090 Å and 0.099 Å respectively for the other two acetic acid molecules. An atom (H4A) is transferred from the carboxylic acid group (atom O5) to the triazine (atom N4) ring. In fact, the C9–N4–N5 angle of the triazine ring in the crystal structure of **3** is 123.3° which correlates with the previously reported values of protonated LTG and with the trend of protonated aminopyridines, that is a larger angle than those of neutral pyridines.[42,54] Thus an acid LTG heterosynthon is formed through the $N^+H\cdots O^-$ charge assisted hydrogen bonding ($N4^+H4A\cdots O5$, N···O 2.719(2) Å, O···H 1.87(2) Å, $N^+H\cdots O^-$ 159(2)°). One trimer is further connected to another by another acid LTG heterosynthon consisting of N–H···O hydrogen bonds ((N1–H1A···O2, N···O 2.808(2) Å, O···H 1.969(1) Å, 164.5(1)°), (N1–H1B···O4, N···O 2.840(2) Å, O···H 2.040(1) Å, 154.4(1)°)) (Fig. 11B). A LTG dimer homosynthon present in the original drug (motif 1) is retained in the LTG layer (N3H3A···N2, N···N 3.137(2) Å, N···H 2.284(1) Å, N–H···N 171.6(1)°) which is sandwiched between two acid layers (Fig. 11C).

The crystal structure of **3** further explains the two step weight loss observed in TGA. The two neutral acetic acid molecules which are bound by the hydrogen bonds in the trimer are released earlier at 75–110 °C (first step weight loss) while the acetate molecule which is bound to the LTG molecule by the stronger ionic hydrogen bond is released at 115–170 °C (second step weight loss).

*(**4**) LTG-4-hydroxy-benzoic acid (1 : 1).* Complex **4** crystallizes in the monoclinic space group $P2_1/c$. The asymmetric unit consists of one LTG cation and one 4-hydroxybenzoate anion.

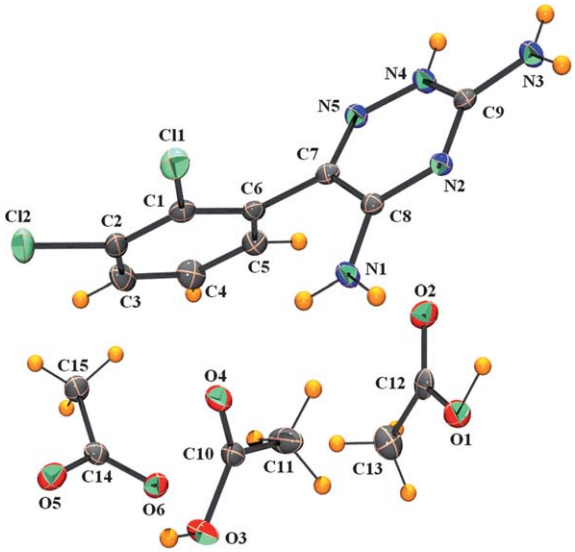

Fig. 10 ORTEP diagram of the asymmetric unit of salt solvate **3** with 50% thermal ellipsoid probability.

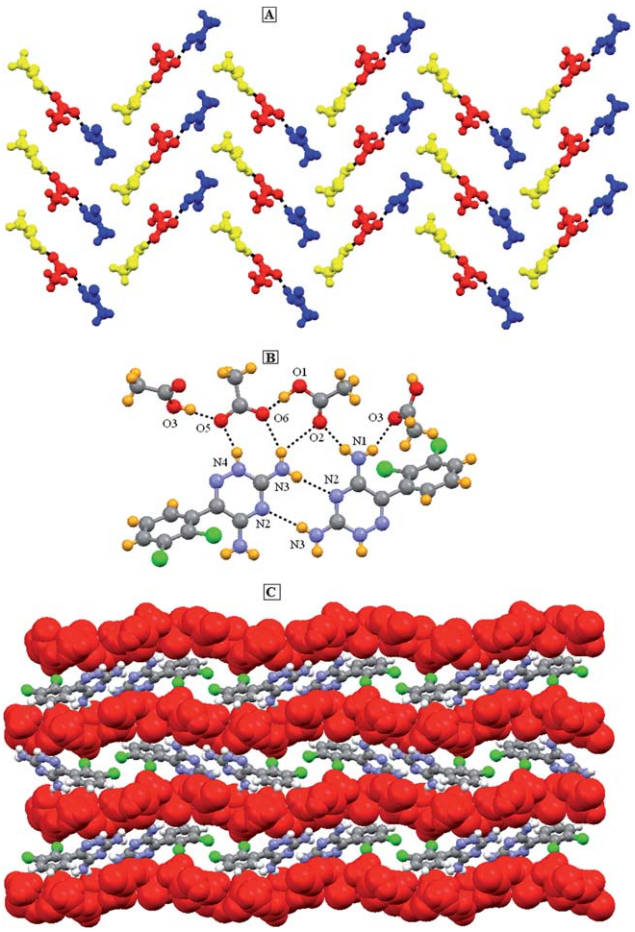

Fig. 11 A) Acetic acid trimer homosynthon layer. (B) Drug dimer homosynthon and drug acid heterosynthons. (C) LTG dimers sandwiched between acetic acid layers.

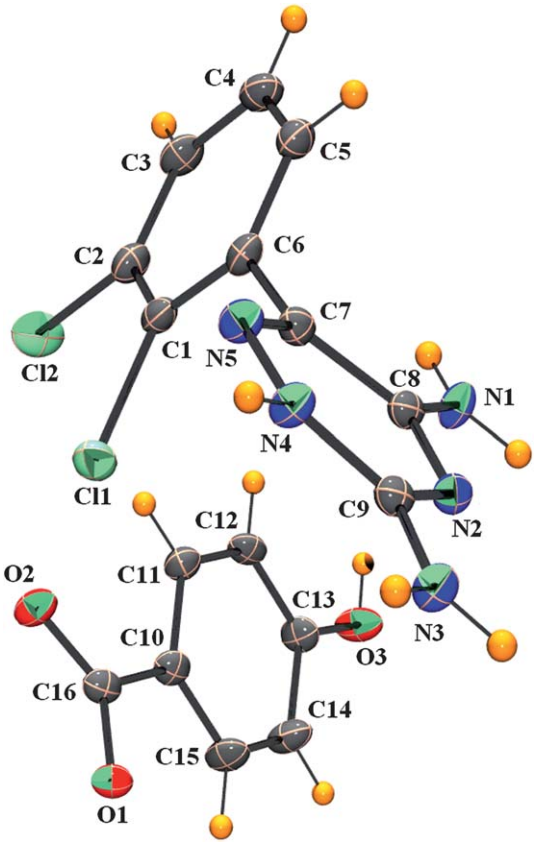

Fig. 12 ORTEP diagram of the asymmetric unit of salt **4** with 50% thermal ellipsoid probability.

Hence this complex can be called a 1 : 1 salt of LTG and 4-hydroxy benzoic acid (Fig. 12). The LTG dimer homosynthon is present in the salt structure (N1–H1A···N2, N···N 2.910(3) Å, N···H 2.063(2) Å, N–H···N 163.1(1)°), but instead of motif 1 in a pure LTG, motif 4 is involved in the formation of the dimeric unit (Fig. 13). The drug dimers are further connected to acid dimers (O3–H3O···O2, O···O 2.642(2) Å, O···H 1.830(1) Å, O–H···O 170.1(1)°) through $N^{+}H\cdots O^{-}$ charge assisted hydrogen bonding ($N4^{+}H4A\cdots O1$, N···O 2.692(2) Å, O···H 1.79(3) Å, $N^{+}H\cdots O^{-}$ 176(3)°) apart from several other N–H···O interactions. Proton transfer is evidenced by the C–O bond distances of

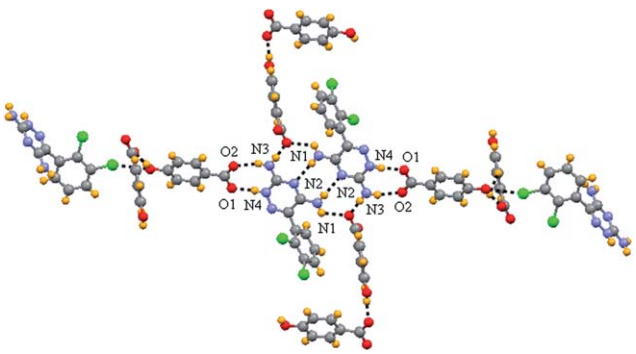

Fig. 13 Basic supramolecular unit showing the 4-HBA dimer and LTG dimer with various weak interactions.

the carboxylate group (with ΔDc–o = 0.022 Å) (Table 4) and the geometry of the LTG triazine ring. The C9–N4–N5 angle of the triazine ring in the crystal structure of **4** is 122.6° which correlates with the previously reported values of protonated LTG.[42] This basic supramolecular unit extends in three dimensions through various other N–H···O hydrogen bonds and Cl···O halogen bonded (2.986(2) Å) interactions (Fig. 13).

Analysis in solution form

Enthalpy of solution. The enthalpy of solution is a direct measurement of heat evolved or taken up when the crystal lattice breaks down in a given solvent.[55] Thus, it is an important inherent thermodynamic parameter to characterize a particular crystal. Scheme 2 explains the enthalpy change accompanying the dissolution of multicomponent crystals. The enthalpy of solution for LTG, all the coformers and their multicomponent forms was determined in a phosphate buffer (pH 7.0) at 37 °C and the results are presented in Table 6. The buffer of pH 7 is selected to ensure that drug (pK_a 5.7) remains in its neutral (unprotonated) form upon dissolution. The enthalpy of solution of LTG and all the coformers except acetic acid is endothermic. It can be seen from Table 6 that dissolution of cocrystals as well as salts also exhibit endothermic behaviour. The molar average enthalpy of the physical mixtures (with the stoichiometry of the multicomponent crystal forms) was calculated utilizing the individual molar enthalpy of solution for the drug and coformer using eqn (1):

$$\Delta_{sol}H_{(cal)} = n_1(\Delta_{sol}H_1) + n_2(\Delta_{sol}H_2) \quad (1)$$

where n_1 and n_2 are the number of moles of the drug and the coformer in the cocrystal/salt. $\Delta_{sol}H_{(cal)}$ is the calculated molar enthalpy of solution of physical mixture. $\Delta_{sol}H_1$ and $\Delta_{sol}H_2$ are the molar enthalpies of solution of the drug and the coformer respectively.

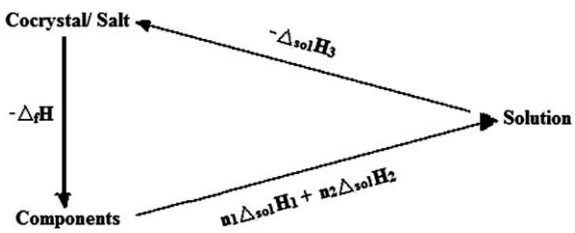

Scheme 2 Thermodynamic cycle representing enthalpies of solution.

Comparison of the experimentally determined enthalpy of solution of multicomponent forms with their calculated molar enthalpy of solution shows that these forms behave more endothermically when compared to the calculated values. The driving force for the formation of these multicomponents is presumably the introduction of additional stabilization by hydrogen bonding and also of Coulombic interactions in the salts. The breaking of these hydrogen bonds, which is an endothermic process, is responsible for their higher endothermic enthalpy of solution than the calculated values. At this point, it is worth mentioning that although the enthalpy of solution for the molecular complexes involves not only the crystal lattice but also the hydration of the components, in the present study, other terms such as primary and secondary solvation are the same for the individual components as well as multicomponent forms. This is because all the experiments have been performed at a constant pH of 7.0, and it is expected that the same molecular species exist for individual components as well as the components after dissolution of molecular complexes. We can determine the enthalpy of formation (Δ_rH) of the cocrystals/salts from their components using eqn (2).

$$\Delta_rH = \Delta_{sol}H_{(cal)} - \Delta_{sol}H_3 \quad (2)$$

where $\Delta_{sol}H_3$ is the experimentally determined molar enthalpy of solution of the cocrystals/salts. The exothermic value of Δ_rH supports the fact that hydrogen bonds between complementary functional groups of different molecules are more favoured than between like molecules of either compound suggesting that these multicomponent forms are thermodynamically favoured. The packing and hydrogen bonding diagrams of various multicomponent forms have been described in the previous section. Table 6 shows the absolute value of Δ_rH at a maximum for compound **3** where one drug molecule is associated with three acetic acid molecules. Higher exothermic enthalpies of formation (Δ_rH) for **3**, **4** and **5** indicate these salts of LTG are more stable than their cocrystals **1** and **2**.

Equilibrium solubility studies. The solubility profiles for all the new phases at various time points in water at 37 °C are shown in Fig. 14 with a comparison to LTG free base. In the free base sample, LTG reached its maximum concentration

Table 6 Molar enthalpy of solution of LTG free base, coformers and their multicomponent forms in phosphate buffer pH 7.0 at 37 °C and the values of Δ_rH

Compound	Molar ratio	$\Delta_{sol}H$/kJ mol^{-1}	$\Delta_{sol}H_{(cal)}$/kJ mol^{-1}	Δ_rH/kJ mol^{-1}	Solubility (s) in phosphate buffer, pH 7.0 (mol L^{-1}) × 10^{-3}
LTG	—	12.37	—	—	1.02
Nicotinamide	—	25.53	—	—	3904.72
1	1 : 1 : 1	52.98	37.90	−15.08	2.81
Acetamide	—	7.14	—	—	7809.45
2	1 : 1	34.19	19.50	−14.68	1.29
Acetic acid	—	−1.70	—	—	—
3	1 : 3	32.52	7.25	−25.27	20.66
4-Hydroxy-benzoic acid	—	19.28	—	—	38.54
4	1 : 1	55.39	31.65	−23.74	2.23
Saccharin	—	4.83	—	—	13.43
5	1 : 1	36.44	17.19	−19.25	3.20

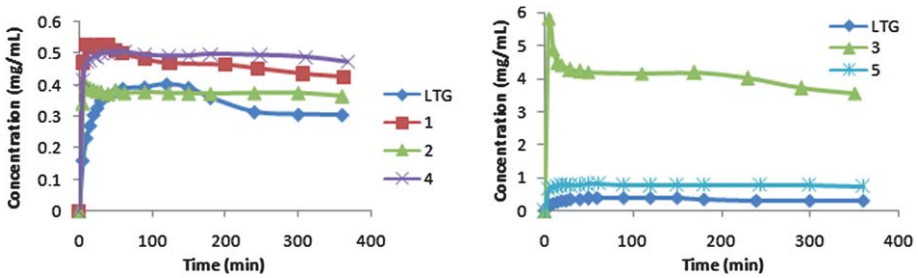

Fig. 14 Solubility studies of LTG free base and its multicomponent forms at various time points in water at 37 °C.

(0.40 mg mL^{-1}) after a time interval of 2 hours while the highest solubility was observed for salt solvate **3** (5.81 mg mL^{-1}) that was attained within 5 minutes followed by a decline over the remaining period of study. This type of solubility profile is displayed by both the cocrystals and solvated salt of acetic acid as cocrystals **1** and **2** also reached the maximum solubility in less than 30 min. However, the salt forms **4** and **5** achieved their maximum concentration in approximately 60 min. The pH of each sample solution was observed during the experiment and has been found to decrease in each case except **2** in contrast with LTG free base (Table 7). In the case of compound **3**, the decrease in pH is significant (from 6.7 to 4.4), which can be attributed to the dissolution of two neutral molecules of acetic acid present as solvent in the crystal structure of **3**. This explains the initial sharp increase in the solubility of this compound. XRPD and DSC analysis of solid residues remaining after the solubility experiment showed that LTG free base, compounds **1** and **2** converted to the LTG hydrate while salt solvate **3** converted to its free salt form upon slurrying in aqueous medium. This explains the decrease in concentration of the drug after an initial rise. These are not isolated cases; there are ample records of cocrystals/solvates reverting back to their free base or hydrates during aqueous solubility studies.[56,57] The salt forms **4** and **5** have been found to be stable during solubility experiments as indicated by XRPD analysis. The solubility (*s*) of LTG in all these multicomponents measured after 24 h of equilibration is given in Table 7. Solubility is a complex parameter that depends upon the enthalpy of fusion, the temperature of solvent and the melting point of the solid.[58] In the present study, we have tried to establish a correlation between melting points and log (*s*) of compounds **3**, **4** and **5** (Table 7). Cocrystals **1** and **2** have not been included in this correlation analysis as these forms exhibit low solubility despite their lower melting points owing to their instability in water. In order to make the correlation more reliable, we included the data from other known complexes of LTG[41] such as LTG hemisuccinate dimethylsulfoxide (DMSO) solvate (**A**), LTG hemifumarate DMSO solvate (**B**) and LTG D, L-hemitartrate DMSO solvate (**C**). A general trend where the higher melting point complexes show lower log (*s*) values is seen, however, this appears as a cluster with one outlying point (**3**) (Fig. 15). Further data in the low melting point region are therefore required to draw any firm conclusions.

Equilibrium solubility studies of LTG in its free base sample and compounds **1–5** were also performed in phosphate buffer at pH 7, 5, 3 and 2 with an aim of determining the effect of pH on the solubility (Fig. 16). As the pH decreases to 2, the solubility of LTG increases up to 4.60 mg mL^{-1} and a similar pattern was observed for cocrystals **1** and **2** (6.67 and 4.63 mg mL^{-1}). Interestingly, the salt forms **3**, **4** and **5** showed an increase in the concentration of drug as the pH is lowered from pH 7 to 5 but started declining as the pH is further decreased to 2 (5.99, 1.30 and 1.74 mg mL^{-1} respectively). These differences in the solubility with varying pH might be due to differences in the sum of free energy of hydration of the species involved in the solubilization process (*i.e.* anions, cations and neutral species that can be present when a salt is dissolved in the aqueous medium).

From the crystal engineering point of view, all the three compounds **2**, **3** and **4** show breaking of motif 2 and exhibit a higher solubility at pH 2 as compared to that in water. However, salt solvate **3** that retained motif 1 exhibited higher solubility than pure LTG while compound **2** that contained motif 3 showed solubility comparable to pure LTG and compound **4**

Table 7 Melting points, solubility and potential conversion of cocrystal/salt during solubility studies in water upon equilibration at 37 °C

Compound	Melting peaks/°C	Solubility (*s*) in water/μg mL^{-1}	log (*s*)	pH of the solution at equilibrium	Conversion during experiment[a]
LTG	217.1	255.2	2.41	6.7	Yes (LTG hydrate)
1	173.9	546.1	2.74	6.6	Yes (LTG hydrate)
2	160.5	320.1	2.51	6.9	Yes (LTG hydrate)
3	170.0	8414.7	3.93	4.4	No
4	234.5	534.8	2.73	5.2	No
5	257.3	696.7	2.84	4.5	No
A[41]	250.0	156.2	2.19	—	—
B[41]	275.0	110.1	2.04	—	—
C[41]	243.0	673.5	2.83	—	—

[a] Conversion assessed by XRPD and DSC. (Compounds **A**, **B** and **C** are added in these data from ref. 41 in order to make the correlation between solubility and melting point more reliable.)

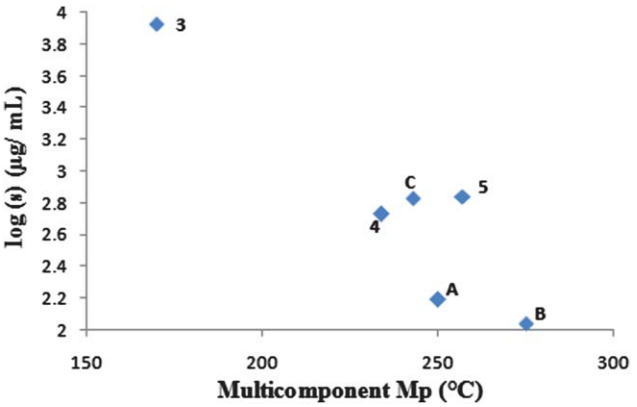

Fig. 15 Log (*s*) as a function of cocrystal/salt melting point.

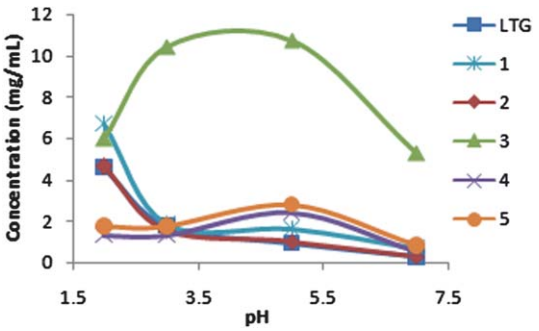

Fig. 16 Solubility of LTG and multicomponent forms **1–5** measured after 24 h of equilibration in phosphate buffers of various pH at 37 °C.

exhibiting motif 4 has been found to be less soluble than pure LTG. These observations are in agreement with Cheney *et al.* who concluded that LTG cocrystal structures that break motif 2 but retain motif 1 are more soluble than pure LTG under acidic conditions while LTG salts that break motif 1 are more soluble than pure LTG in aqueous solutions.[42]

Stability studies. The physical stability of multicomponent forms of LTG was investigated at 25 °C/60% RH for one month. The DSC of these samples did not show any additional peaks indicating these to be stable which is further confirmed by the absence of any significant changes in their XRPD patterns.

Animal activity studies. In the MES test, LTG and all the compounds tested produced a dose dependent abolition of hind limb extension in mice. Results are presented as median effective doses (ED_{50} in mg kg^{-1}) required to protect 50% of animals tested against MES-induced seizures. ED_{50} values determined in mice (Fig. 17) following oral administration showed compounds **1**, **3** and **5** to be effective even at a lower dose of 2.5 mg kg^{-1} while compound **4** achieved similar potency at a dose of 5.0 mg kg^{-1} as compared to compound **2** and LTG free base which abolished the HLE only at a dose of 7.5 mg kg^{-1} and above. All these compounds showed a pattern of absorption quite similar to that observed in the solubility studies. Thus, this study illustrates that pharmaceutical cocrystals and salts can significantly alter the dosage profile of parent drug in animal activity studies.

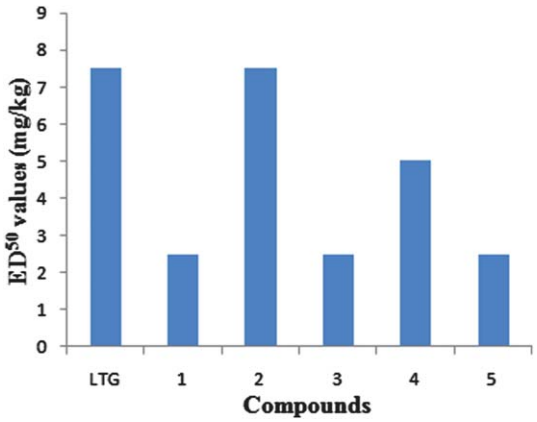

Fig. 17 ED_{50} values (mg kg^{-1}) of LTG in a pure commercial sample and its multicomponents.

Conclusion

The work discussed herein illustrates the successful and methodical implementation of the multicomponent approach (cocrystals and salts) for improving the physicochemical properties of LTG. The formation of new solid phases in each case was indicated by DSC, whereas the preliminary differentiation between cocrystals and salts was performed by FT-IR analysis. The single crystal structure for the cocrystal with acetamide and salts with acetic acid and 4-hydroxy-benzoic acid was determined. In the cocrystal **2**, LTG exhibits an aminopyridazine dimer homosynthon (motif 3) which is linked to the acetamide dimer homosynthon through a N–H···O hydrogen bond. In the crystal structures of salts **3** and **4**, the aminopyridine dimer of LTG is retained but with slight deviations in the geometry in the case of compound **4** (motif 4). In all these three structures motif 2 was broken. Solution calorimetry suggested compounds **3**, **4** and **5** to be thermodynamically more stable forms as compared to **1** and **2**. The cocrystals **1** and **2** were found to convert into LTG hydrate, salt solvate **3** converted to its pure salt form while salts **4** and **5** are found to be stable during solubility studies. Maximum enhancement in aqueous solubility has been observed in salt solvate **3**, which is found to be stable and has significantly lowered the dosage profile of LTG in animal activity studies. Thus, this multicomponent form **3** can be considered for further development. Some other coformers are also under investigation in our laboratory for exploring more cocrystals and salts of this drug and will constitute our future communication.

Acknowledgements

We gratefully acknowledge the funding provided by the UGC (Research Fellowship for Meritorious Students), New Delhi, India.

References

1 S. Datta and D. J. W. Grant, *Nat. Rev. Drug Discovery*, 2004, **3**, 42–57.
2 C. B. Aakeroy, M. E. Fasulo and J. Desper, *Mol. Pharmaceutics*, 2007, **4**, 317–322.
3 P. V. Arnum, *Pharm. Technol.*, 2010, **2**, 50–56.

4 C. Leuner and J. Dressman, *Eur. J. Pharm. Biopharm.*, 2000, **50**, 47–60.
5 J. C. Chaumeil, *Exp. Clin. Psychopharmacol.*, 1998, **20**, 211–215.
6 K. Kawakami, N. Oda, K. Miyoshi, T. Funaki and Y. Ida, *Eur. J. Pharm. Sci.*, 2006, **28**, 7–14.
7 D. Singhal and W. Curatolo, *Adv. Drug Delivery Rev.*, 2004, **56**, 335–347.
8 A. Abdalla and K. Mäder, *Eur. J. Pharm. Biopharm.*, 2007, **66**, 220–226.
9 K. Uekama, F. Hirayama and T. Irie, *Chem. Rev.*, 1998, **98**, 2045–2076.
10 J. Hecq, M. Deleers, D. Fanara, H. Vranckx and K. Amighi, *Int. J. Pharm.*, 2005, **299**, 167–177.
11 S. L. Morissette, O. Almarsson, M. L. Peterson, J. F. Remenar, M. J. Read, A. V. Lemmo, S. Ellis, M. J. Cima and C. R. Gardner, *Adv. Drug Delivery Rev.*, 2004, **56**, 275–300.
12 A. T. M. Serajuddin, *Adv. Drug Delivery Rev.*, 2007, **59**, 603–616.
13 S. M. Berge, L. D. Bighley and D. C. Monkhouse, *J. Pharm. Sci.*, 1977, **66**, 1–19.
14 A. T. M. Serajuddin and M. Pudipeddi, Salt Selection Strategies, in *Handbook of Pharmaceutical Salts: Properties, Selection and Use*, 2002, pp. 135–160.
15 R. Banerjee, P. M. Bhatt, N. V. Ravindra and G. R. Desiraju, *Cryst. Growth Des.*, 2005, **5**, 2299–2309.
16 L. D. Bighley, S. M. Berge and D. C. Monkhouse, Salt Forms of Drugs and Absorption, in *Encyclopedia of Pharmaceutical Technology*, 1996, vol. 13, pp. 453–499.
17 W. Q. Tong and G. Whitesell, *Pharm. Dev. Technol.*, 1998, **3**, 215–223.
18 N. Schultheiss and A. Newman, *Cryst. Growth Des.*, 2009, **9**, 2950–2967.
19 K. Shiraki, N. Takata, R. Takano, Y. Hayashi and K. Terada, *Pharm. Res.*, 2008, **25**, 2581–2592.
20 A. Bak, A. Gore, E. Yanez, M. Stanton, S. Tufekcic, R. Syed, A. Akrami, M. Rose, S. Surapaneni, T. Bostick, A. King, S. Neervannan, D. Ostovic and A. Koparkar, *J. Pharm. Sci.*, 2008, **97**, 3942–3956.
21 J. Lu and S. Rohani, *Org. Process Res. Dev.*, 2009, **13**, 1269–1275.
22 D. J. Good and N. Rodriguez-Hornedo, *Cryst. Growth Des.*, 2009, **9**, 2252–2264.
23 M. K. Stanton and A. Bak, *Cryst. Growth Des.*, 2008, **8**, 3856–3862.
24 J. F. Remenar, S. L. Morissette, M. L. Peterson, B. Moulton, J. M. Macphee, H. R. Guzman and O. Almarsson, *J. Am. Chem. Soc.*, 2003, **125**, 8456–8457.
25 S. Basavoju, D. Bostrom and S. P. Velaga, *Pharm. Res.*, 2008, **25**, 530–541.
26 N. Shan and M. Zaworotko, *Drug Discovery Today*, 2008, **13**, 440–446.
27 A. V. Trask, *Mol. Pharmaceutics*, 2007, **4**, 301–309.
28 *The Internet Drug Index*, www.rxlist.com/cgi/generic/lamotrigine.htm, accessed 13 November, 2009.
29 K. R. Parmar, K. A. Patel, S. R. Shah and N. R. Sheth, *J. Inclusion Phenom. Macrocyclic Chem.*, 2009, **65**, 263–268.
30 (*a*) *GRAS Notices*, http://www.cfsan.fda.gov/rdb/opa-gras.html; (*b*) *Food additive status list*, http://www.cfsan.fda.gov/~rdb/opa-appa.html.
31 B. Sridhar and K. Ravikumar, *Acta Crystallogr., Sect. E: Struct. Rep. Online*, 2005, **61**, o3805–o3807.
32 R. W. Janes, *J. Chem. Crystallogr.*, 1999, **29**, 163–167.
33 R. B. Parthasaradhi, R. K. Rathnakar, R. R. Raji, R. D. Muralidhara, and R. K. S. Chander, *US. Pat.*, 2005/0119265 A1, 2005.
34 B. Sridhar and K. Ravikumar, *Acta Crystallogr., Sect. E: Struct. Rep. Online*, 2006, **62**, o4752–o4754.
35 R. W. Janes, J. N. Lisgarten and R. A. Palmer, *Acta Crystallogr., Sect. C: Cryst. Struct. Commun.*, 1989, **45**, 129–132.
36 M. Kubicki and P. W. Codding, *J. Mol. Struct.*, 2001, **570**, 53–60.
37 B. Sridhar and K. Ravikumar, *Mol. Cryst. Liq. Cryst.*, 2007, **461**, 131–141.
38 D. A. Sawyer and F. C. Copp, *US. Pat.*, 4847249, 1989.
39 B. Potter, R. A. Palmer, R. Withnall, M. J. Leach and B. J. Chowdhry, *J. Chem. Crystallogr.*, 1999, **29**, 701–706.
40 B. Sridhar and K. Ravikumar, *Acta Crystallogr., Sect. C: Cryst. Struct. Commun.*, 2009, **65**, o460–o464.
41 J. Galcera and E. Molins, *Cryst. Growth Des.*, 2009, **9**, 327–334.
42 M. L. Cheney, N. Shan, E. R. Healey, M. Hanna, L. Wojtas, M. J. Zaworotko, V. Sava, S. Song and J. R. Sanchez-Ramos, *Cryst. Growth Des.*, 2010, **10**, 394–405.
43 A. A. Miller, P. Wheatley, D. A. Sawyer, M. G. Baxter and B. Roth, *Epilepsia*, 1986, **27**, 483–489.
44 Oxford Diffraction, *CrysAlis PRO CCD and CrysAlis PRO RED*, Oxford diffraction Ltd, Yarnton, England, 2009.
45 G. M. Sheldrick, *Acta Crystallogr., Sect. A: Found. Crystallogr.*, 2008, **64**, 112–122.
46 L. J. Farrugia, *J. Appl. Crystallogr.*, 1999, **32**, 837–838.
47 L. J. Farrugia, *J. Appl. Crystallogr.*, 1997, **30**, 565.
48 *POV-Ray, version 3.6*, Chemical Crystallography Laboratory, Australia.
49 A. L. Spek, *J. Appl. Crystallogr.*, 2003, **36**, 7–13.
50 C. F. Macrae, I. J. Bruno, J. A. Chisholm, P. R. Edgington, P. McCabe, E. Pidcock, L. Rodriguez-Monge, R. Taylor, J. van de Streek and P. A. Wood, *J. Appl. Crystallogr.*, 2008, **41**, 466–470.
51 S. L. Childs, G. P. Stahly and A. Park, *Mol. Pharmaceutics*, 2007, **4**, 323–338.
52 M. Hanna, N. Shan and M. L. Cheney, Thor Pharmaceutics, *WO Pat.*, 2009/061513 A1, 2009.
53 V. R. Hathwar and T. N. Guru Row, *J. Phys. Chem. A*, 2010, **114**, 13434–13441.
54 R. A. Palmer, B. S. Potter, M. J. Leach and B. Z. Chowdhury, *J. Chem. Crystallogr.*, 2007, **37**, 771–777.
55 P. G. Royall and S. Gaisford, *Curr. Pharm. Biotechnol.*, 2005, **6**, 215–222.
56 S. L. Childs, L. J. Chyall, J. T. Dunlap, V. N. Smolenskaya, B. C. Stahly and G. P. Stahly, *J. Am. Chem. Soc.*, 2004, **126**, 13335–13342.
57 D. P. McNamara, S. L. Childs, J. Giordano, A. Iarriccio, J. Cassidy, M. S. Shet, R. Mannion, E. O'Donnell and A. Park, *Pharm. Res.*, 2006, **23**, 1888–1897.
58 A. Martin, J. Newburger and A. Adjei, *J. Pharm. Sci.*, 1980, **69**, 487–491.

